An analysis of the vortex street generated in a viscous fluid

By JOHN W. SCHAEFER* AND SALAMON ESKINAZI
Syracuse University, Syracuse, New York

(Received 26 December 1958)

An analytic solution for the velocity field of a vortex street generated in a viscous fluid is developed. A method is presented for the determination of the true transverse spacing of vortices. Experimental geometry and velocity data, obtained by hot-wire techniques, are presented.

The experimental results verified the validity of the analytic solution. The vortices of a real viscous vortex street were found to resemble very closely the exponential solution of the Navier–Stokes equations for an isolated axisymmetric rectilinear vortex. Three basic regions of vortex street behaviour were apparent at each Reynolds number investigated—a 'formation region' in which the vortex street is developed and large dissipation of vorticity occurs, a 'stable region' in which the vortices display a stable periodic laminar regularity, and an 'unstable region' in which the street disappears and turbulence develops. Geometry and velocities were determined.

1. Introduction

The periodicity in wakes in the form of discrete vortices at an intermediate range of Reynolds number ($R = U_0 d/\nu$, where U_0 is the free-stream velocity, d the cylinder diameter and ν kinematic viscosity) has been recognized for many years. In the lower portion of this range, $40 < R < 125$, there exists an ordered and stable wake—a vortex system commonly referred to as the Kármán vortex street.

Academic and practical interest in the vortex street phenomenon has resulted in many theoretical and experimental investigations of the vortex system generated behind a two-dimensional bluff obstacle. This available literature concerning viscous vortex streets may best be summarized as descriptive but incomplete analytically. As pointed out by Rosenhead (1953), a quantitative theoretical treatment which will consolidate the facts already available is needed.

The purpose of this investigation is the development of an analytic solution for the velocity field of a viscous vortex street and the accurate determination of street geometry. An experimental analysis was performed to support and verify the analytic results.

Most of the experimental results on this subject were obtained through photographs of the streak-lines developed by colour dyes or suspensions in the fluid.

* Now at Lewis Research Center, National Aeronautics and Space Administration, Cleveland, Ohio.

In most instances careful precautions were taken to photograph a steady flow by moving the camera with the fluid. Since vortices move at a relative velocity to the free stream, the apparent centres of the vortices as observed in the photograph are then centres of zero relative velocity and not the centres of maximum vorticity. Hooker (1936) used this argument to show the reasons for great discrepancies in the measurements of street geometry. Tyler (1930) applied the hot-wire technique for measurements of velocity in the Kármán street. Since then this technique has become very productive for measurements of velocity and geometry of the vortex street. The results presented here have been obtained with the hot-wire technique.

2. Analytic considerations

The solution of the Navier–Stokes equations for a viscous vortex system is not available in its general form. It is the interest of this investigation to rely on a mathematical description of a viscous vortex street based on linearizing methods which allow superposition of solutions. The basic solution of the Navier–Stokes equations for an isolated rectilinear viscous vortex growing in time due to viscosity will be considered as the elemental vortex in the superposition method.

The isolated viscous vortex

The Navier–Stokes equations in vorticity form for a two-dimensional flow field in the (x, y)-plane is

$$\frac{D\zeta}{Dt} = \nu\left\{\frac{\partial^2\zeta}{\partial x^2} + \frac{\partial^2\zeta}{\partial y^2}\right\}, \tag{1}$$

where ζ is the vorticity and ν is the kinematic viscosity. In the case of isolated rectilinear vortices, equation (1) reduces to

$$\frac{\partial\zeta}{\partial t} = \nu\left\{\frac{\partial^2\zeta}{\partial r^2} + \frac{1}{r}\frac{\partial\zeta}{\partial r}\right\}, \tag{2}$$

where r is the radial distance from the axis of rotation. Therefore, for an isolated rectilinear vortex initially of strength $\Gamma_0/2\pi$ concentrated along the axis of rotation, the vorticity at a time t and any position r is given by

$$\zeta = \frac{\Gamma_0}{4\pi\nu t}\exp\left(-\frac{r^2}{4\nu t}\right). \tag{3}$$

The circulation around a circle of radius r is

$$\Gamma = \int_0^{2\pi} v_\theta r\, d\theta = \int_0^{2\pi}\int_0^r \zeta r\, d\theta\, dr = \Gamma_0\left[1 - \exp\left(-\frac{r^2}{4\nu t}\right)\right], \tag{4}$$

where θ is the polar angle; and therefore the circumferential velocity of the vortex is

$$v_\theta = \frac{\Gamma}{2\pi r} = \frac{\Gamma_0}{2\pi r}\left[1 - \exp\left(-\frac{r^2}{4\nu t}\right)\right]. \tag{5}$$

For vanishing viscosity and time, or for large r, the solution reduces to that for a potential vortex. Equation (5) is plotted in figure 2.

The potential vortex street

The co-ordinates appropriate to the following theory, as shown in figure 1, are explained below. The co-ordinate x is the distance downstream from the tripping cylinder to the point in the flow field $P(x, y)$ under study. The co-ordinate s is the distance in the x-direction from the nearest vortex to the left of P to the

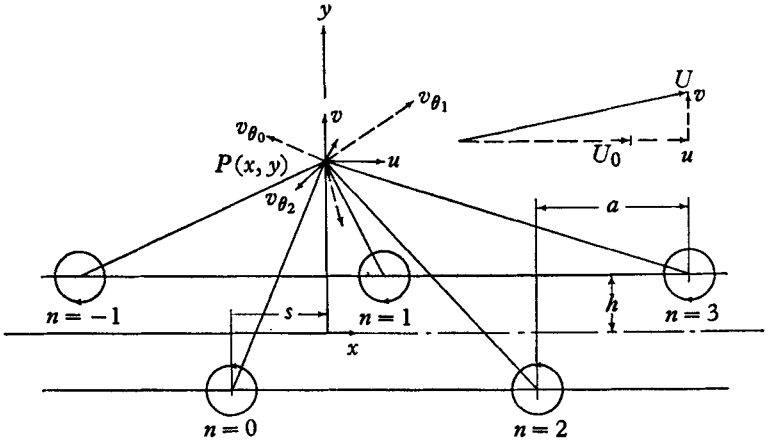

FIGURE 1. Idealized vortex street; geometry and co-ordinates.

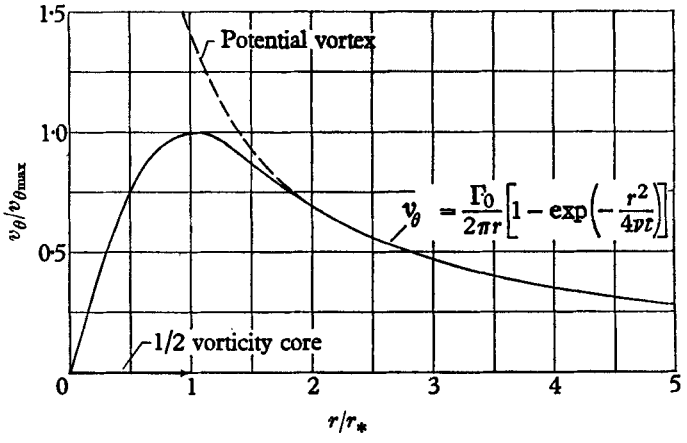

FIGURE 2. Peripheral velocity of an isolated vortex.

point P. This vortex, to the left of P, is considered the reference vortex $n = 0$. The indice n represents any other vortex a distance na in the x-direction away from the reference vortex. Negative n indicates a vortex to the left of P; positive n to the right of P. Therefore, the term $(x-s+na)$ is the distance from the tripping cylinder to any vortex. Similarly, $(x-s+na)/2af$ is the time in the life of any vortex from its generation at the tripping cylinder, f being the frequency of vortex shedding. The equations developed below are therefore valid for $-\infty < y < \infty$ and for half a cycle, i.e. $0 < s < a$.

In this co-ordinate representation, the velocity components for an idealized potential Kármán street of an infinite extent are given by the following summations:

$$\left.\begin{aligned} u &= \frac{\Gamma}{2\pi}\sum_{\pm n=0}^{\infty}(-1)^{|n|}\frac{y-(-1)^{|n|}h}{[|n|\,a\mp s]^2+[y-(-1)^{|n|}h]^2},\\ v &= \frac{\Gamma}{2\pi}\sum_{\pm n=0}^{\infty}\pm(-1)^{|n|}\frac{|n|\,a\mp s}{[|n|\,a\mp s]^2+[y-(-1)^{|n|}h]^2}. \end{aligned}\right\} \tag{6}$$

Here h is the transverse distance from the street centreline to the path of the vortex centres. Each term in the summation is of the type

$$u=\frac{\Gamma}{2\pi}\frac{y'}{r^2}\quad\text{and}\quad v=\frac{\Gamma}{2\pi}\frac{x'}{r^2},$$

where x', y' and r are co-ordinates from the axis of an isolated vortex. Equations (6) may be altered to represent the solution for a finite, variable-geometry vortex street. This is accomplished by limiting the number of terms of the summation and replacing h and a by h_n and a_n where h_n and a_n are functions of the vortex position.

The viscous vortex street

Hooker (1936) presented an analysis in which only the vortex nearest the point of interest was considered viscous. Since the peripheral velocity outside the vorticity core varies as $1/r$, a viscous vortex behaves essentially as a potential vortex outside the core. Therefore, vortices far from the point of interest may be considered as potential vortices. This method, therefore, suggests essentially a potential street of vortices with a single viscous vortex described by equation (5) replacing the potential vortex nearest the point of interest.

A more general solution for a finite, viscous, variable-geometry vortex street was developed from equations (6). After incorporating the decay term of each vortex as given by equation (5) and the variable geometry h_n (a is a constant with distance downstream at a given Reynolds number as determined experimentally) the velocity components are

$$\left.\begin{aligned} u &= \frac{\Gamma_0}{2\pi}\sum_{\pm n=0}^{k}\left[\left\{(-1)^{|n|}\frac{y-(-1)^{|n|}h_n}{[|n|\,a\mp s]^2+[y-(-1)^{|n|}h_n]^2}\right\}\right.\\ &\qquad\left.\times\left\{1-\exp\left(-\frac{[|n|\,a\mp s]^2+[y-(-1)^{|n|}h_n]^2}{4\nu[(x-s+na)/2af]}\right)\right\}\right],\\ v &= \frac{\Gamma_0}{2\pi}\sum_{\pm n=0}^{k}\left[\left\{\pm(-1)^{|n|}\frac{|n|\,a\mp s}{[|n|\,a\mp s]^2+[y-(-1)^{|n|}h_n]^2}\right\}\right.\\ &\qquad\left.\times\left\{1-\exp\left(-\frac{[|n|\,a\mp s]^2+[y-(-1)^{|n|}h_n]^2}{4\nu[(x-s+na)/2af]}\right)\right\}\right]. \end{aligned}\right\} \tag{7}$$

For a finite street, the limit of summation k is not necessarily the same for positive and negative n.

Equations (7) reduce to Hooker's solution if $k=\infty$, $h_n=$ const., and $n=0$ in the decay term only.

Because of an absence of *a priori* knowledge of Γ_0, equations (7) are more useful in the following dimensionless form, for which the diameter d of the tripping cylinder is used as reference length:

$$\left.\begin{aligned} q_x &= \sum_{\pm n=0}^{k}\left[\left\{(-1)^{|n|}\frac{\dfrac{y}{d}-(-1)^{|n|}\dfrac{h_n}{d}}{\left[|n|\dfrac{a}{d}\mp\dfrac{s}{d}\right]^2+\left[\dfrac{y}{d}-(-1)^{|n|}\dfrac{h_n}{d}\right]^2}\right\}\right. \\ &\qquad\left.\times\left\{1-\exp\left(-\frac{\left[|n|\dfrac{a}{d}\mp\dfrac{s}{d}\right]^2+\left[\dfrac{y}{d}-(-1)^{|n|}\dfrac{h_n}{d}\right]^2}{4\nu\left[\dfrac{(x-s+na)/d}{2(a/d)fd^2}\right]}\right)\right\}\right], \\ q_y &= \sum_{\pm n=0}^{k}\left[\left\{\pm(-1)^{|n|}\frac{|n|\dfrac{a}{d}\mp\dfrac{s}{d}}{\left[|n|\dfrac{a}{d}\mp\dfrac{s}{d}\right]^2+\left[\dfrac{y}{d}-(-1)^{|n|}\dfrac{h_n}{d}\right]^2}\right\}\right. \\ &\qquad\left.\times\left\{1-\exp\left(-\frac{\left[|n|\dfrac{a}{d}\mp\dfrac{s}{d}\right]^2+\left[\dfrac{y}{d}-(-1)^{|n|}\dfrac{h_n}{d}\right]^2}{4\nu\left[\dfrac{(x-s+na)/d}{2(a/d)fd^2}\right]}\right)\right\}\right] \end{aligned}\right\} \tag{8}$$

where $q_x = 2\pi ud/\Gamma_0$ and $q_y = 2\pi vd/\Gamma_0$.

This viscous vortex street solution was obtained from the superposition of the solutions of equation (2) for the velocity distribution of isolated axisymmetric viscous vortices. The correlation of analytic and experimental results indicates that equation (5) represents very closely the peripheral velocity of a vortex in a viscous vortex street. This fact justifies the assumed axial symmetry of the vortices. The results of Timme (1957) also substantiate this conclusion. Therefore, superposition affords a very close approximation of the actual flow conditions of a viscous vortex street. At downstream positions very close to the generating cylinder, the results of this theory are in relatively poorer agreement with the actual conditions because of the immediate proximity of the cylinder and because of the rolling-up process of the vortex sheet into fully-developed vortices.

The method of analysis is represented in figures 1 and 3.

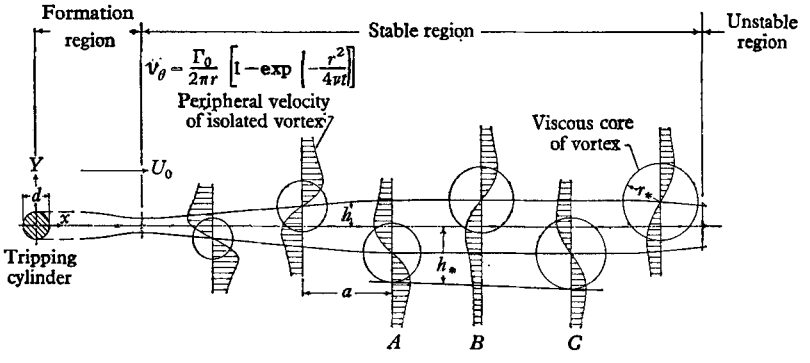

FIGURE 3. Vortex street configuration at $R = 62$, velocity and geometry to scale.

3. Method of evaluation of the velocity field

The determination of the vortex street velocities, as given by equations (8), requires an accurate knowledge of the basic geometric parameters including the extent of the street. These parameters have been determined experimentally and analytically.

The longitudinal spacing was determined experimentally, as will be described in § 4. In the fully developed stable vortex street, this spacing was found to be constant with x for a given Reynolds number. The periodicity was determined from the velocity fluctuation oscillogram and was also found to be constant with x for the fully developed street at a given Reynolds number. The initial time in the life of a vortex was assumed to be at $x = 0$, the axis of the tripping cylinder. Therefore, as indicated in the velocity equations, the life of the vortex n is $t = (x - s + na)/2af$.

In a viscous vortex, the vorticity is concentrated in a finite circular core which grows with time according to equation (3). The outer boundary of the core is defined as $r = r_*$, this value of r being where the velocity is a maximum as shown in figure 2. This value as determined by differentiation of equation (5) is given by

$$\frac{r_*^2}{4\nu t} = 1{\cdot}26.$$

The dimensionless core radius r_*/d, which grows with time, is given by

$$\frac{r_*}{d} = \sqrt{\left(5{\cdot}04\frac{\nu t}{d^2}\right)}. \tag{9}$$

A preliminary analysis indicated that the maximum velocity fluctuation does not occur along the path of vortex centres as some experimenters have asserted. An analysis based on the configuration of a general vortex street, as in figure 3, demonstrated that the maximum velocity fluctuation occurs in the immediate neighbourhood of the core edge farthest from the street centreline. As shown in figure 3, let h_* be that distance from the street centreline, and let us visualize a hot wire at some point along the path of h_*. When vortices A and C pass the hot-wire location, they will induce their maximum peripheral velocity on the hot wire. However, when vortex B is directly above the hot wire, it will induce a weaker velocity in the opposite direction. By varying the position of the hot wire from h_* to any y, it can be observed from figure 3 that the magnitude of fluctuation within a cycle will decrease when the hot wire is moved in either direction. Then the y-location of the maximum induced velocity variation is in the neighbourhood of h_*. This fact was verified in the analysis. The position of maximum fluctuating velocity is easily determined experimentally, and since it occurs very near the outer edge of the vortex core, the dimensionless path of vortex centres h/d is therefore given by

$$\frac{h}{d} = \frac{h_*}{d} - \frac{r_*}{d}. \tag{10}$$

The value of the viscosity required for the determination of r_*/d, in equation (9), was taken as the molecular viscosity since the wake may be described as in

a state of laminar oscillation. Also Timme (1957) has shown that in the Reynolds number range for which a stable vortex street exists, the molecular viscosity determines the decay process.

Upon determination of the geometry, time and extent of the vortex street, the numerical solution for the velocity field relative to the free-stream velocity was determined from equations (7) and (8). Since the initial circulation Γ_0 is an unknown parameter, the velocity field was computed in terms of the dimensionless velocity q_x and q_y. The solutions describe the dimensionless velocity

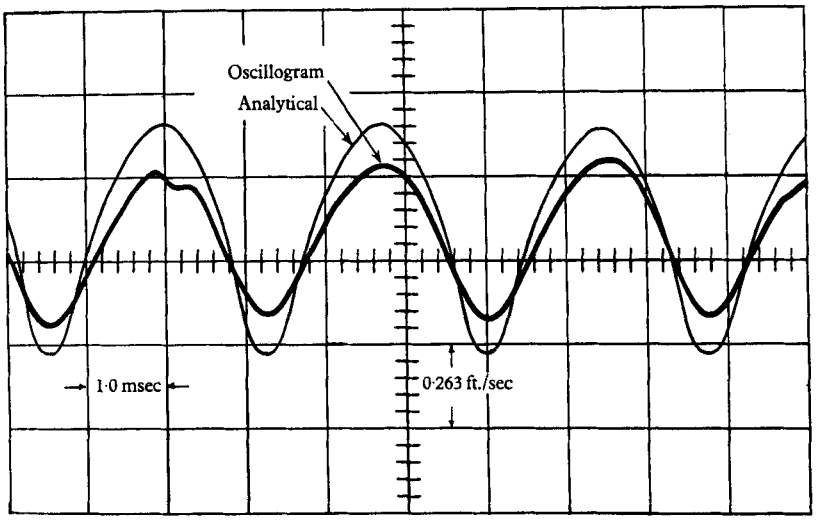

FIGURE 4. Velocity fluctuation at $R = 62$, $x/d = 10$, $y/d = 0$.

distribution of a vortex street generated behind a cylinder moving with a velocity of Q_0 in a still fluid. If a dimensionless free-stream velocity of Q_0 is superposed on the above solutions, the flow of a fluid about a stationary cylinder is achieved. Therefore, the dimensionless total velocity vector is

$$\mathbf{Q} = \mathbf{Q}_0 + \mathbf{q}, \tag{11}$$

where $\mathbf{q} = \mathbf{i}q_x + \mathbf{j}q_y$ and $\mathbf{Q}_0 = 2\pi\mathbf{i}U_0 d/\Gamma_0$. Since Γ_0 is unknown, the analytic solution was matched to the experimental results at a point in the flow field in order to determine Q_0. The match point was taken at $x/d = 10$, $y/d = 0$ for a Reynolds number of 62, the only Reynolds number at which the analysis was performed. The dimensionless free-stream velocity was determined by satisfying the relation $Q_T/Q_0 = U_T/U_0$ at the match point (Q_T and U_T denote time averages of Q and U). The time average of $\mathbf{q}$ from equation (11) was also matched at that point using (8). Q_0 was determined from the known terms Q_T/Q_0 and $Q_T - Q_0$.

At any desired point in the flow field $P(x, y)$, the velocity was determined from equation (11) by substitution of the results of equations (8) for varying s and the determined value of Q_0. A plot of the velocity over a cycle gave Q_T at the point, and also the root-mean-square value $\tilde{q}'_T$ and peak-to-peak value $\hat{q}'_T$ of the fluctuating component of velocity q'. A comparison of analytic and experimental results is presented in figures 4 to 12 and table 1.

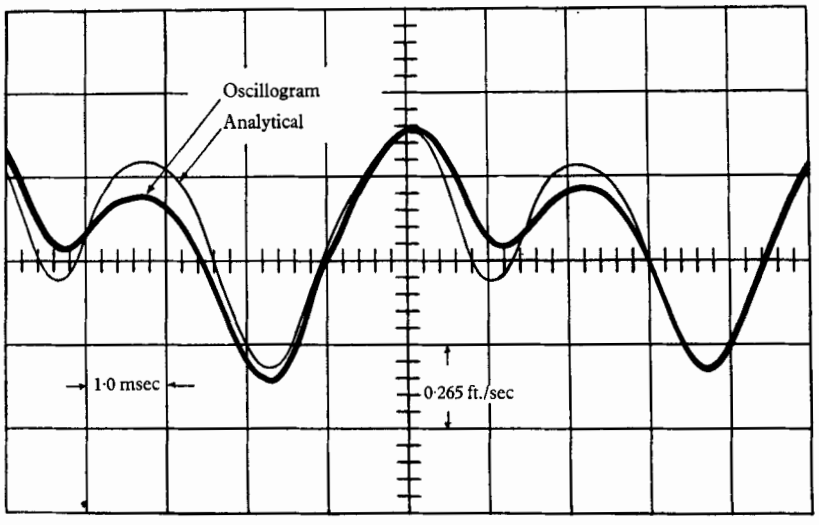

FIGURE 5. Velocity fluctuation at $R = 62$, $x/d = 10$, $y/d = 0{\cdot}429$.

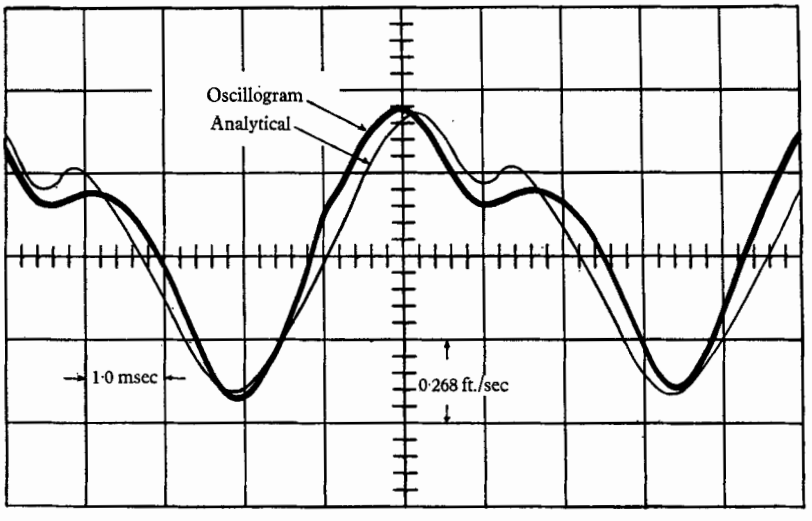

FIGURE 6. Velocity fluctuation at $R = 62$, $x/d = 10$, $y/d = 0{\cdot}857$.

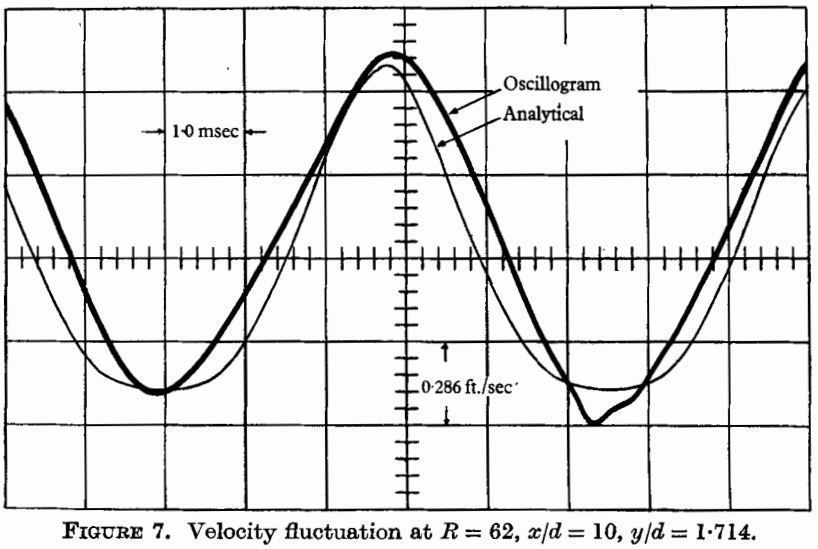

FIGURE 7. Velocity fluctuation at $R = 62$, $x/d = 10$, $y/d = 1{\cdot}714$.

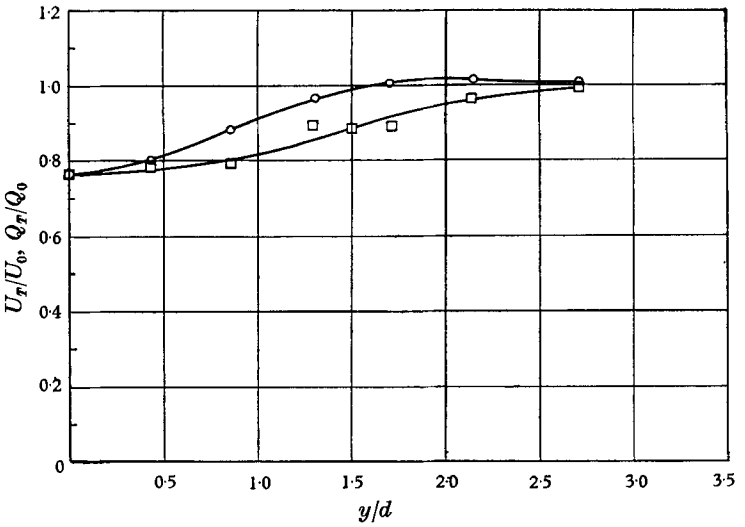

FIGURE 8. Time average total velocity, $R = 62$, $x/d = 10$. ○, Analytic; □, experimental.

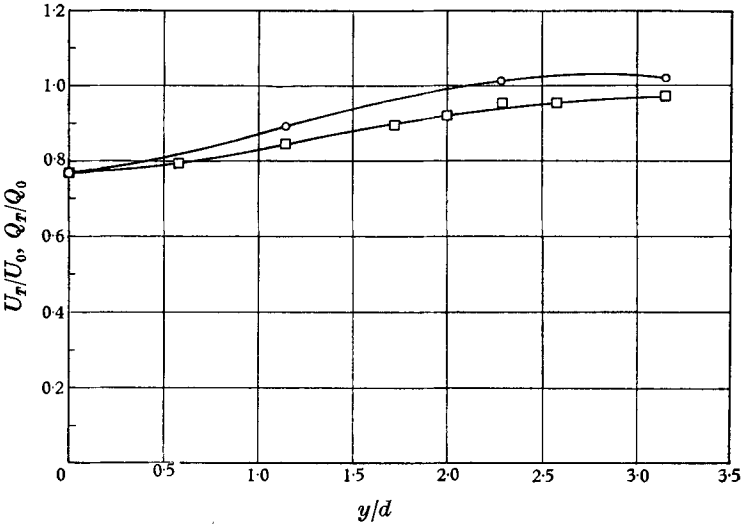

FIGURE 9. Time average total velocity, $R = 62$, $x/d = 20$. ○, Analytic; □, experimental.

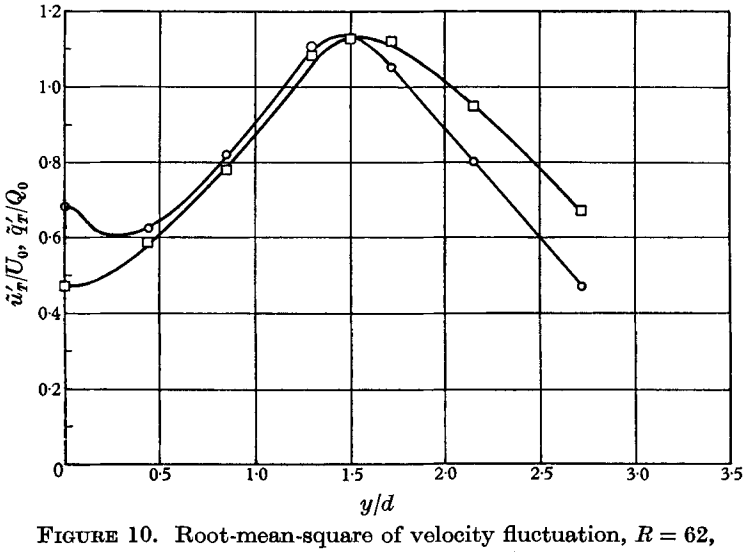

FIGURE 10. Root-mean-square of velocity fluctuation, $R = 62$, $x/d = 10$. ○, Analytic; □, experimental.

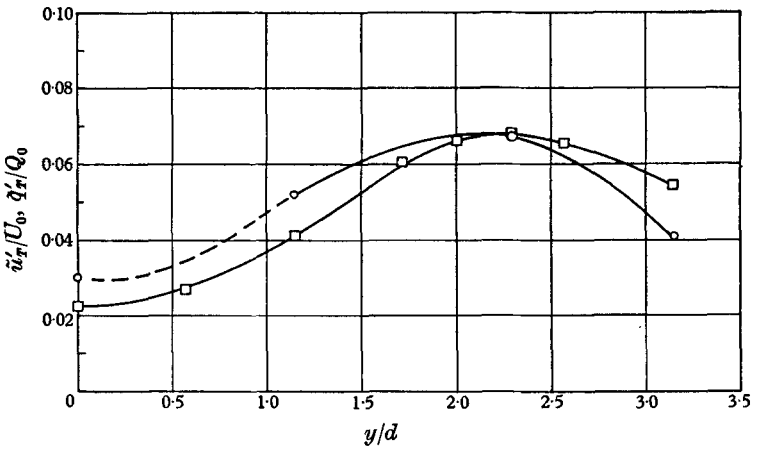

FIGURE 11. Root-mean-square of velocity fluctuation, $R = 62$, $x/d = 20$.
○, Analytic; □, experimental.

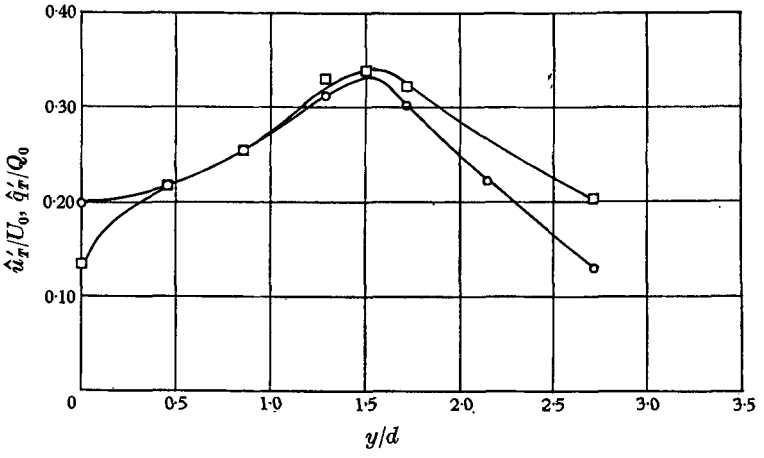

FIGURE 12. Peak-to-peak velocity fluctuation, $R = 62$, $x/d = 10$.
○, Analytic; □, experimental.

x/d	y/d	U_T/U_0	Q_T/Q_0	$\tilde{u}'_T/U_0$	$\tilde{q}'_T/Q_0$	$\hat{u}'_T/U_0$	$\hat{q}'_T/Q_0$
10	0	0·762	0·762	0·047	0·068	0·132	0·198
	0·429	0·782	0·799	0·059	0·062	0·216	0·216
	0·857	0·793	0·886	0·078	0·082	0·253	0·254
	1·286	0·892	0·968	0·109	0·110	0·331	0·312
	1·714	0·892	1·006	0·112	0·105	0·323	0·302
	2·143	0·964	1·018	0·095	0·080	0·279	0·222
	2·714	0·997	1·014	0·067	0·047	0·202	0·130
20	0	0·760	0·772	0·022	0·030	—	—
	1·143	0·843	0·891	0·041	0·052	—	—
	2·286	0·951	1·010	0·068	0·067	—	—
	3·143	0·971	1·021	0·054	0·041	—	—

TABLE 1. Comparison of analytic and experimental velocities, $R = 62$

4. Experimental procedures

A hot-wire anemometer was used for all velocity and geometry measurements because of its high sensitivity, reliability and its convenience in determining the desired results. The constant-current hot-wire set, built at Syracuse University, was similar to the set used by Eskinazi & Yeh (1956).

The vortex street system was generated in a circular low-turbulence wind tunnel of diameter 18 in. with a continuously variable flow velocity from 0 to 20 ft. sec. A tripping cylinder of circular cross-section generated the vortex street. The cylinder was mounted in a traversing mechanism for variation of longitudinal distance from the hot wire. The cylinders used were 0·035 and 0·080 in. piano wire; all data presented here were obtained with the 0·035 in. diameter tripping cylinder.

Vortices are shed from a tripping cylinder at a definite shedding frequency depending on Reynolds number; this frequency is preserved throughout the stable region of a street. Therefore, the cyclic variation of velocity at a fixed point is very stable and consistent for moderate Reynolds numbers. The hot wire, positioned at a fixed point $P(x, y)$, recorded the cyclic variation in time or s. The hot wire was positioned parallel to the axis of rotation of the vortices; therefore, the velocity vector was at all times on a plane perpendicular to the axis of the hot wire. The hot wire therefore responded to the total velocity vector.

The mean voltage across the hot wire determined the temporal mean velocity. The cyclic voltage fluctuation from the hot wire was compensated for the heat capacity lag. The magnitude and wave forms of the velocity fluctuations were determined respectively from a root-mean-square voltmeter and a dual channel oscilloscope. Since the street periodicity was never in excess of 800 c/s, an electrical filter with flat response to 1000 c/s was used to eliminate amplifier noise in the measured signals.

The spacing h_* was determined from the plots of the root-mean-square fluctuating velocity (a plot of peak-to-peak fluctuating velocity yields the same h_*). The spacing h_* is essential in determining the path of vortex centres as outlined previously. This spacing should not be confused with h, the transverse spacing of the path of vortex centres.

The longitudinal spacing a was determined with a special hot-wire system. Two hot wires were fixed at a known longitudinal distance apart. The longitudinal spacing was computed from the phase angle between the two fluctuating hot-wire signals and the known distance between the hot wires.

The hot-wire material was tungsten of 0·00015 in. diameter. The central sensing portion was of approximately $\frac{1}{16}$ in. length; the ends were copper plated for soldering to the probe needle points.

A sensitive alcohol micromanometer was used for pressure measurements. The free-stream velocity head was sensed by a total pressure probe in the flow and a static pressure tap at the wall. The mouth of the total pressure probe was of a high aspect ratio rectangular cross-section to eliminate the necessity of corrections due to viscous effects at low velocities.

5. Results and discussion

Comparison of analytic and experimental velocity

A comparison of analytic and experimental results was performed at $x/d = 10$ and 20 and $R = 62$ for all comparable velocity variables. The analytic velocity fluctuation wave forms are plotted to scale on the experimental oscillograms in figures 4 to 7. Comparison of time average total velocities U_T/U_0 and Q_T/Q_0 are presented in figures 8 and 9, root-mean-square velocity fluctuation $\tilde{u}'_T/U_0$ and $\tilde{q}'_T/Q_0$ in figures 10 and 11 and peak-to-peak velocity fluctuation $\hat{u}'_T/U_0$ and $\hat{q}'_T/Q_0$ in figure 12.

The analytic results demonstrate favourable agreement with the actual experimental flow conditions. The favourable comparison allows the following conclusions:

(1) The vortices of the real vortex street behave approximately according to equations (4) and (5).

(2) The vortex street analysis of equations (7) is a good approximation of actual conditions.

(3) The radius of the vortex core is closely determined by equation (9), and the outer edge of the core is very nearly coincident with the position of maximum velocity fluctuation.

(4) The transverse spacing of vortices is closely determined by equation (10).

(5) The assumed origin of time, $x = 0$, is justified.

The greatest discrepancy in the comparison of results is in the time average total velocity. This discrepancy appears to be primarily due to experimental error in measurement of U_T/U_0. The analysis below supports this observation. The carrier velocity of vortices in the street U_V may be determined experimentally in two ways:

$$U_V = 2fa, \tag{12}$$

and

$$U_V = U_T + |(\mathbf{u}' + \mathbf{v}')|_{s=0}. \tag{13}$$

The result of equation (12) for $R = 62$ is $U_V/U_0 = 0{\cdot}92$. Based on the position of the vortex centre in the analytic wave form, the experimental value from equation (13) is $U_V/U_0 = 0{\cdot}85$ approximately. Since the values of a and f substituted in equation (12) correlate well with those of other experimenters, the value $U_V/U_0 = 0{\cdot}92$ is reasonably accurate. Experimental results for U_T therefore appear to be lower than the true value. This discrepancy was estimated to be partially due to the non-linear effect of large velocity fluctuation on the measured time average total velocity U_T. It is also interesting to note that the largest discrepancy occurs in the region of largest velocity fluctuation. From the analysis shown in figure 19, the vortex carrier velocity is given by $Q_V/Q_0 = 0{\cdot}91$, which is in good agreement with equation (12).

Circulation

The dimensionless free-stream velocity determined from the match of analytic and experimental results is $Q_0 = 2{\cdot}565$. Therefore, from the definition of Q_0, the total circulation of a vortex in the fully developed state is

$$\Gamma_0 = 2\pi d U_0/Q_0 = 0{\cdot}0261 \text{ ft.}^2/\text{sec.}$$

From boundary-layer theory, the rate K at which vorticity in the form of vortex sheets is generated at the tripping cylinder is given by

$$K = \frac{d\Gamma}{dt} = \frac{d}{dt}\iint_A \zeta dx dy = \Lambda U_0^2,$$

where Λ is defined as

$$\Lambda = \frac{1}{U_0^2}\frac{d}{dt}\iint_A \zeta dx dy,$$

and U_0 is the free-stream velocity just outside the boundary layer (see Birkhoff & Zarantonello 1957). In the case when $v = 0$,

$$\Lambda = \frac{1}{U_0^2}\int u\frac{\partial u}{\partial y}dy.$$

For a laminar parabolic boundary layer, $\Lambda = 0{\cdot}5$. Assuming that vorticity is conserved in the rolling-up to form vortices, the rate of generation of vorticity may be written also as

$$K = \Gamma_0 f.$$

Substituting the experimental conditions and the circulation of this investigation, we get $\Lambda = 0{\cdot}343$ and therefore

$$\Gamma_0 = \frac{0{\cdot}343U_0^2}{f}.$$

The result of this investigation based on the fully developed street gives a smaller value of Λ than that analytically predicted by the laminar parabolic boundary-layer theory. It is therefore apparent that vorticity is partly lost in the rolling-up to form fully developed vortices. As presented by Birkhoff (1953), an empirical analysis by Prandtl substantiates this finding. Prandtl determined that the initial vorticity decreases to about half where the first vortex centres appear.

Solving for Λ from the experimental results of Timme (1957) at a Reynolds number of 200 (moving cylinder in still water), we find $\Lambda = 0{\cdot}46$. The discrepancy in Λ is attributed to the difference in vorticity dissipation in the two experiments. It is also of interest to note that, as determined by Roshko (1953), $R = 200$ is in a Reynolds number range ($150 < R < 300$) in which considerable experimental scatter occurs due to instability of the wake.

Geometry

The longitudinal spacing a of the stable vortex street is constant at a given Reynolds number as shown in figure 13 for four Reynolds numbers. This fact has been well substantiated by other investigations, i.e. Taneda (1955), Goldstein (1943) and Roshko (1953). The variation of longitudinal spacing with Reynolds number is presented in figure 14. The results of Taneda (1955), for experiments in water for a large range of Reynolds numbers, agree very well with the results of this investigation. Taneda's results are also plotted, together with the results of this investigation and that of Timme. The results of the empirical analysis developed below are also presented.

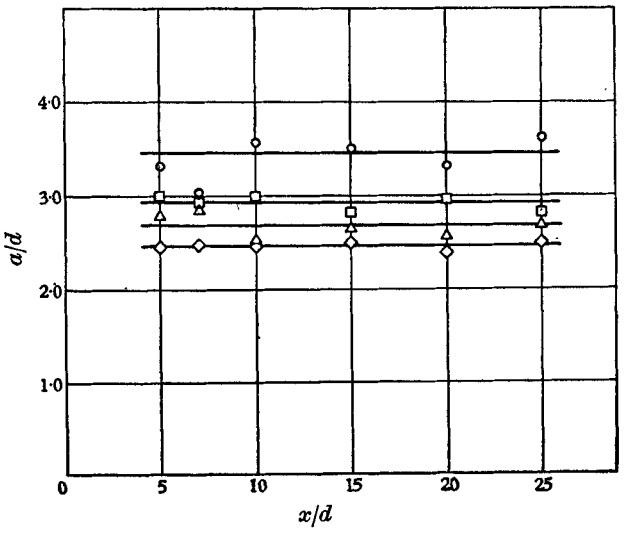

FIGURE 13. Longitudinal spacing versus distance downstream. ○, $R = 59$; □, $R = 75$; △, $R = 98$; ◇, $R = 122$.

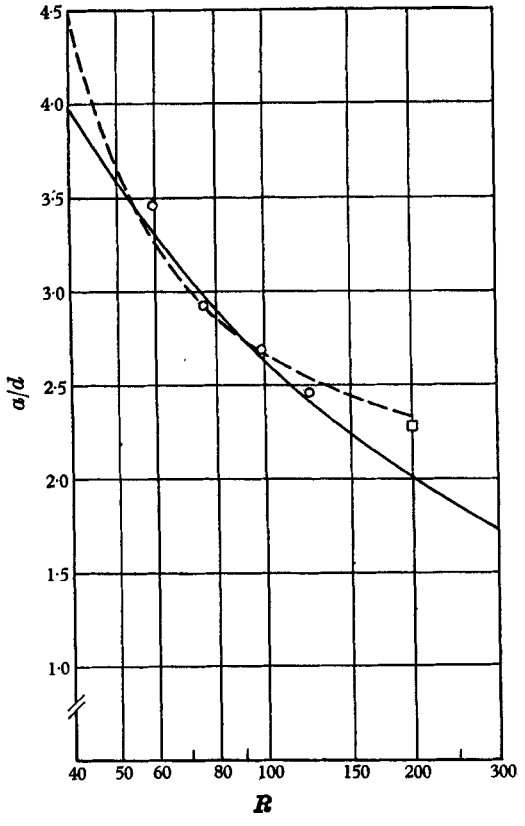

FIGURE 14. Summary of longitudinal spacing results. —, Taneda, experimental; – – –, equation (14); □, Timme; ○, Schaefer and Eskinazi.

An interesting empirical result may be derived from the determined longitudinal spacing. From equation (12) for the carrier velocity of vortices,

$$\frac{a}{d} = \frac{U_V}{2fd}.$$

If $U_V = C_V U_0$, where C_V is assumed tentatively to be independent of Reynolds number, then

$$\frac{a}{d} = \frac{C_V U_0}{2fd} = \frac{C_V}{2S} = \frac{C_V R}{2F},$$

where S is the Strouhal number fd/U_0 and F the dimensionless frequency fd^2/ν. The empirical results of Kovasznay (1949) and Roshko (1953), valid for $40 < R < 150$, also agree with the results of this investigation; they found $S = 0{\cdot}212(1 - 21{\cdot}2R^{-1})$, which is the same as $F = 0{\cdot}212R - 4{\cdot}5$, and the substitution of this into the above equation gives

$$\frac{a}{d} = \frac{C_V R}{0{\cdot}424R - 9{\cdot}0}. \tag{14}$$

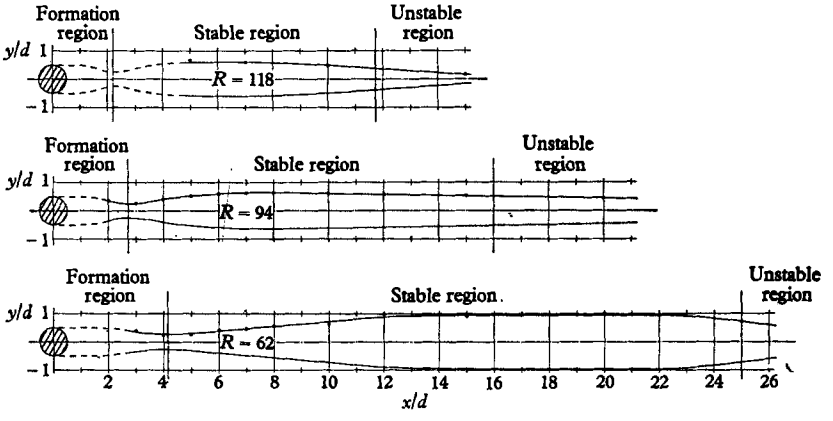

FIGURE 15. Transverse spacing for three Reynolds numbers.

With the determined value of C_V, equation (14) is plotted in figure 14 as a function of Reynolds number. The good agreement of experimental results and equation (14) indicates that U_V/U_0 is dependent of R and that its value is close to 0·90 in the stable range of the street.

The variation of transverse spacing with distance downstream for three Reynolds numbers is shown in figure 15. A tabulation of all transverse spacing parameters h_*/d, r_*/d, and h/d is presented in table 2. As seen in figure 15, the path of vortex centres exhibits similar variation at all Reynolds numbers investigated. A necking-down in h/d is apparent at a short distance from the tripping cylinder; this is followed by an increase to a maximum value; h/d then decreases at large distances from the tripping cylinder. Goldstein (1943) postulates a similar downstream variation, and states that upon formation of the vortex street the distance between rows increases until a position of transitional stability is reached at which time there is no further increase; the increase in core radius

then becomes the dominating factor and the stable system tends to close up and disappear.

At each Reynolds number (figure 15), the x/d distance at which the minimum spread of the path of centres occurs near the tripping cylinder is nearly coincident with the position of maximum downstream velocity fluctuation. This position is defined as the start of the fully developed street. The region between the tripping cylinder and this minimum point is therefore referred to as the 'formation region'.

Reynolds number	x/d	h_*/d	r_*/d	h/d	h/a
62	3	0·91	0·51	0·40	0·12
	4	0·83	0·59	0·24	0·07
	5	0·91	0·65	0·26	0·08
	6	1·14	0·72	0·42	0·13
	7	1·26	0·78	0·48	0·15
	8	1·40	0·83	0·57	0·18
	10	1·57	0·93	0·64	0·20
	12	2·00	1·01	0·99	0·30
	15	2·03	1·12	0·91	0·28
	20	2·31	1·31	1·00	0·31
	25	2·17	1·46	0·71	0·22
94	2	0·71	0·36	0·35	0·13
	3	0·70	0·44	0·26	0·10
	4	0·91	0·51	0·40	0·15
	5	1·09	0·57	0·52	0·19
	6	1·22	0·63	0·59	0·22
	7	1·31	0·68	0·63	0·23
	8	1·37	0·72	0·65	0·24
	10	1·41	0·81	0·60	0·22
	12	1·46	0·88	0·58	0·22
	15	1·51	0·98	0·53	0·20
	20	1·59	1·14	0·45	0·18
118	5	1·17	0·50	0·67	0·27
	7	1·20	0·60	0·60	0·24
	10	1·21	0·71	0·50	0·20
	15	1·03	0·87	0·16	0·06

TABLE 2. Transverse spacing parameters and spacing ratio

At large distances behind the tripping cylinder the vortex street exhibits an unstable behaviour. This instability becomes apparent approximately at the downstream position where the vorticity core extends to the path of centres of the opposite row; i.e. $h/d = r_*/2d$. The region in which $h/d < r_*/2d$ is therefore termed the 'unstable region'. The region of the stable vortex street, between the 'formation region' and 'unstable region' is referred to as the 'stable region'.

The regions are shown in figure 15. The start of the stable region is governed approximately by the empirical relation

$$R\left(\frac{x}{d}\right)_f \doteqdot 260,$$

where $(x/d)_f$ is the distance downstream at which the stable region begins. The end of the stable region is governed approximately by the relation

$$R\left(\frac{x}{d}\right)_s \doteqdot 1500,$$

where $(x/d)_s$ is the distance downstream at which the stable region ends.

The formation region is characterized by the development of the stable vortex street and dissipation of vorticity as previously mentioned. Kovasznay (1949) observed the existence of the formation region in his investigation. He states that in the formation of a vortex street vortices are not shed directly from the tripping cylinder but develop some distance downstream as an instability in the laminar wake.

The unstable region is characterized by irregular behaviour and the eventual transition to turbulence. Taneda (1955) observed two possible phenomena in this region, one a transition to turbulence and the other the eventual formation of a vortex street of large scale. Goldstein (1943) mentions only the former characteristic.

A number of other experimenters have attempted to measure transverse spacing. Tyler (1930), in his hot-wire experiments, assumed the incorrect relation $h/d = h_*/d$. Photographic techniques have been applied by other experimenters in which the point of zero velocity was assumed to be the vortex centre. Hooker (1936) pointed out that this assumption was incorrect; the point of maximum vorticity which is the vortex centre is not coincident with the point of zero velocity. This fact is apparent from figure 19. Timme's experimental and analytic results also substantiate this fact.

The variation of the spacing ratio h/a as defined in this investigation, with distance downstream at a given Reynolds number is proportional to h, since the longitudinal spacing is a constant. The maximum spacing ratios are approximately equal to the value predicted by Kármán (1912), $h/a = 0{\cdot}281$, in his idealized analysis. From the plots of h/d and a/d, it was found that $(h/a)_{\max} = 0{\cdot}28$ at $R = 62$ and $(h/a)_{\max} = 0{\cdot}24$ at $R = 94$ and 118. The experimental values are tabulated in table 2. Other experimenters have observed large values up to 0·525; it is believed that these large values are due to the previously mentioned incorrect methods of determining the transverse spacing.

Velocity

The variation of the time average of total velocity U_T/U_0 with distance from the vortex street centreline is presented in figure 16 for a number of downstream positions. The transverse variation of velocity deficiency $U_{T_{\max}} - U_T$ is compared with an exponential decay as shown in figure 17. The normalized variables are the local velocity deficiency divided by the maximum velocity deficiency, and $b_{\frac{1}{2}} = 1$ where $\Delta U_T/\Delta U_{T_{\max}} = 0{\cdot}5$.

The variation of fluctuating velocity $\tilde{u}'_T/U_0$ with distance from the street centreline is presented in figure 18 for a number of downstream positions and a Reynolds number of 62. The position in y/d of the maximum peak-to-peak velocity fluctuation is essentially coincident with the position of maximum root-mean-square of velocity fluctuation in all cases.

The velocity fluctuation wave forms at $x/d = 10$ are presented at various transverse locations in figures 4 to 10. Some low-amplitude wave forms exhibit a small 'pip' on the signal—this is hot-wire bridge noise and is not instability

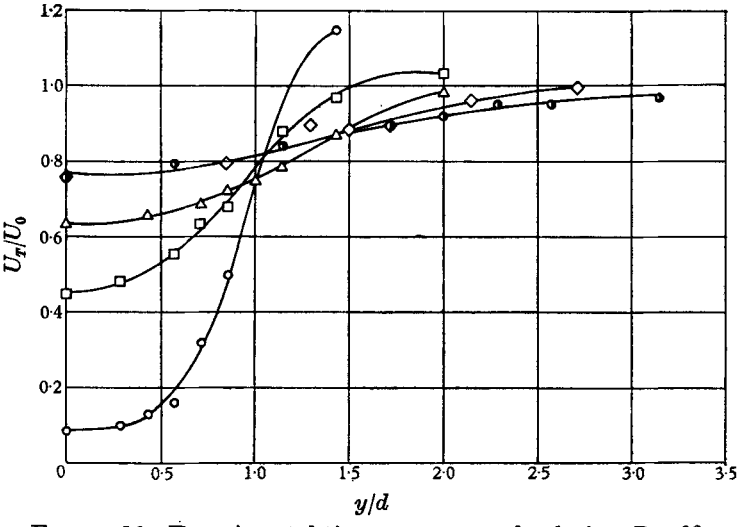

FIGURE 16. Experimental time average total velocity, $R = 62$.
○, $x/d = 2$; □, $x/d = 4$; △, $x/d = 6$; ◇, $x/d = 10$; ◑, $x/d = 20$.

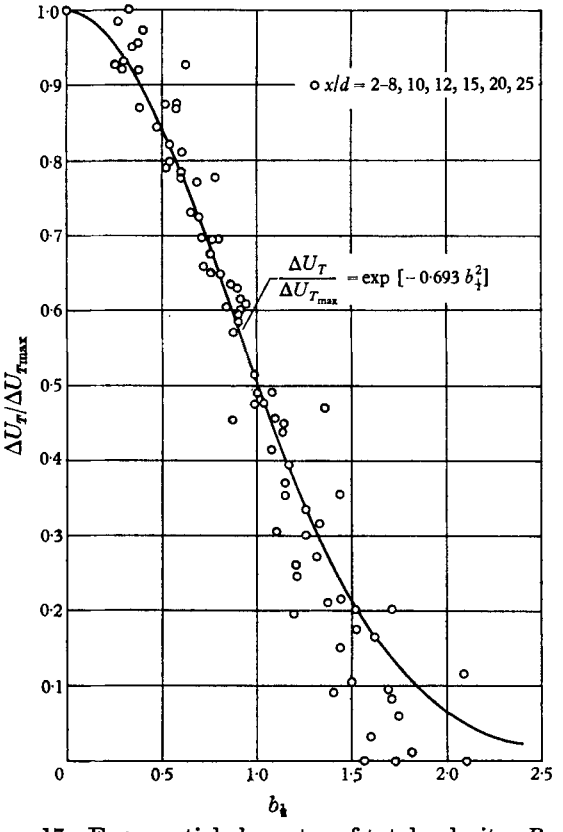

FIGURE 17. Exponential character of total velocity, $R = 62$.

in the vortex street. The wave forms at $y/d = 0$ exhibit a frequency double that of the shedding frequency because of the equal influence of the symmetrically staggered rows.

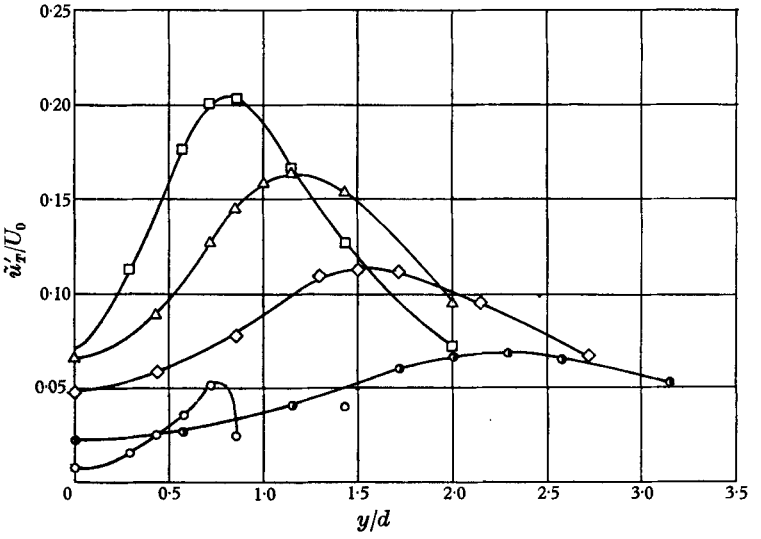

FIGURE 18. Experimental root-mean-square of velocity fluctuation, $R = 62$. ○, $x/d = 2$; □, $x/d = 4$; △, $x/d = 6$; ◇, $x/d = 10$; ◑, $x/d = 20$.

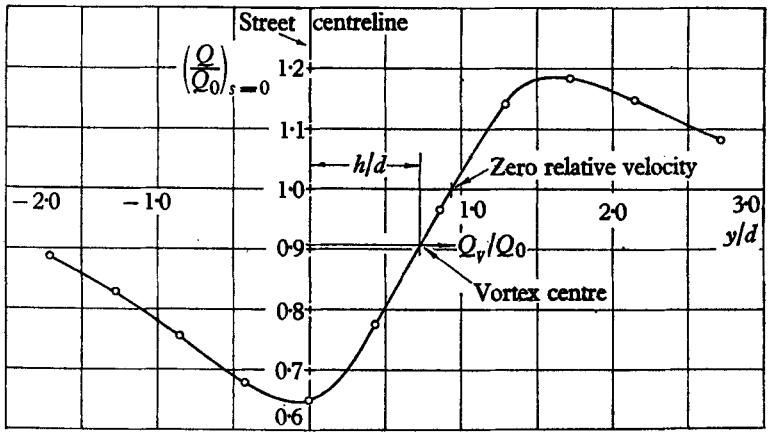

FIGURE 19. Analytic transverse velocity variation through a vortex, $R = 62$, $x/d = 10$.

No quantitative analysis of vortex street velocity at Reynolds numbers higher than 122 was undertaken in this investigation. However, a number of observations are of interest. Above a Reynolds number of approximately 125, occasional irregular behaviour was apparent at all downstream locations. The rate of occurrence and randomness of these disturbances increased with increasing Reynolds number. A low frequency 'whip' of the whole vortex street at large distances downstream was also apparent. The amplitude of the whip increased with increasing Reynolds number.

6. Conclusions

The vortex street generated behind a circular obstacle is essentially composed of vortices which behave according to the solution for an isolated viscous vortex, equations (4) and (5), as presented in figure 2. The velocity at any point in the stable vortex street wake relative to free stream is the summation of the velocity contributions at the point from all vortices.

The vortex street phenomenon in the Reynolds number range $50 < R < 125$ may be divided into three distinct areas of behaviour, the 'formation', 'stable' and 'unstable' regions as shown in figure 15. The formation region is the region immediately behind the tripping cylinder in which the vortex street develops and a dissipation of vorticity occurs. The stable region is the region of the fully developed stable vortex street in which the vortices display a periodic laminar regularity. The unstable region is the region far downstream which exhibits irregular behaviour and the eventual transition to turbulence. Above a Reynolds number of approximately 125, a completely stable vortex street is not apparent.

The transverse spacing is accurately determined by equation (10).

A large velocity deficiency, a backflow, exists directly behind the tripping cylinder. The amplitude of velocity fluctuation at the start of the stable region may be as great as 75 % of the average velocity.

REFERENCES

BIRKHOFF, G. 1953 Formation of vortex streets. *J. Appl. Phys.* **24**, 98–103.

BIRKHOFF, G. & ZARANTONELLO, E. H. 1957 *Jets, Wakes, and Cavities*, pp. 283, 284. New York: Academic Press.

ESKINAZI, S. & YEH, H. 1956 An investigation on fully developed turbulent flows in a curved channel. *J. Aero. Sci.* **23**, 23–35.

GOLDSTEIN, S. 1943 *Modern Developments in Fluid Dynamics*, vol. II, pp. 553–71. Oxford University Press.

HOOKER, S. G. 1936 On the action of viscosity in increasing the spacing ratio of a vortex street. *Proc. Roy. Soc.* A, **154**, 67–89.

VON KÁRMÁN, T. & RUBACH, H. 1912 Über den Mechanismus des Flussigkeits- und Luftwiderstandes. *Phys. Z.* **13**, 49–59.

KOVASZNAY, L. S. G. 1949 Hot-wire investigation of the wake behind cylinders at low Reynolds numbers. *Proc. Roy. Soc.* A, **198**, 175–90.

LAMB, H. 1945 *Hydrodynamics*, 6th ed., p. 578. Dover Publications.

MILNE-THOMSON, L. M. 1955 *Theoretical Hydrodynamics*, pp. 541, 542, 360. London: Macmillan Co.

ROSENHEAD, L. 1953 Vortex systems in wakes. *Advanc. Appl. Mech.* vol. III, pp. 185–95. New York: Academic Press.

ROSHKO, A. 1953 On the development of turbulent wakes from vortex streets. *NACA TN* 2913.

SCHLICHTING, H. 1955 *Boundary Layer Theory*. New York: McGraw-Hill.

TANEDA, S. 1952 Studies on wake vortices (II), experimental investigation of the wake behind cylinders and plates at low Reynolds numbers. *Res. Inst. Appl. Mech.*, Vol. I, pp. 29–40.

TIMME, A. 1957 Über Die Geschwindigkeitsverteilung in Wirbeln. *Ingen. Archiv*, Bd XXV, pp. 205–25.

TYLER, E. 1930 A hot-wire method for measurement of the distribution of vortices behind obstacles. *Phil. Mag.* (7), **9**, 1113–30.